

Modeling of Parametrically Excited Microelectromechanical Oscillator Dynamics with Application to Filtering

Barry DeMartini*, Jeff Moehlis*, Kim Turner*, Jeffrey Rhoads†, Steve Shaw†, and Wenhua Zhang*

*Department of Mechanical and Environmental Engineering, University of California, Santa Barbara, California 93106–5070, Email: baredog@enr.ucsb.edu

†Department of Mechanical Engineering, Michigan State University, East Lansing, Michigan 48824–1226, Email: rhoadsje@msu.edu

Abstract—A model for the dynamics of an emerging class of electrostatically driven microelectromechanical oscillators, parametrically excited MEM oscillators, has been developed. The equation of motion for these devices is a nonlinear version of the Mathieu Equation, which gives rise to rich dynamics. A standard perturbation analysis, averaging, has been adopted to analyze this complicated system. Numerical bifurcation analysis was employed and successfully verified these analytical results. Using the analytical and numerical tools developed for this model, along with the experimental results for such a device, parameters for the system are identified. This model is a pivotal design tool for the development of parametrically excited MEM filters.

I. INTRODUCTION

Parametric amplification has increased sensitivity in many common MEMS devices: cantilevers [1], [2], torsional oscillators [3], and translational oscillators [4], [5]. Some of the current applications exploiting parametric resonance include: mass sensing [5], scanning tunneling microscopy and atomic force microscopy [3], and signal filtering [6]. Beneficial to these applications is the unique ability of such oscillators to remain quiescent outside the region of parametric excitation and transition sharply to large amplitude oscillatory motion at the edge of the stability boundaries. Due to the presence of time varying stiffness terms in the equation of motion, such devices experience parametric resonances when driven at frequencies close to $2\omega_o/n$, where n is an integer greater than or equal to one and ω_o is the natural frequency [7]. In the aforementioned studies, as in the present study, the dominant parametric regime occurs when driving the device near twice the natural frequency, i.e., $n = 1$, which will be the region studied here.

Commonly studied forms of the Mathieu Equation involve linear time varying stiffness terms, e.g. [8]. The present work builds on the recent work in [9], [5], and [10], wherein the equations exhibit both linear and nonlinear parametric excitation. As a result of these additional terms, the nonlinear behavior of the system's response takes on a much more complicated form, where hardening, softening, and mixed nonlinearities occur depending on driving voltage. In this section the governing dynamics, analytical procedure, and

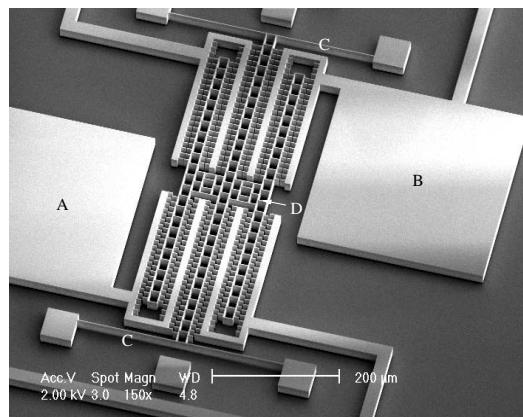


Fig. 1. Scanning electron microscope image of a representative parametrically excited MEMS oscillator.

numerical bifurcation analysis (used to verify analytical results) are reviewed. Section II highlights the process used for the identification of system parameters and possible future improvements to create a more accurate model. The current model and analytical tools have been utilized to aid in the development of parametrically excited MEMS filters.

A. Governing Dynamics

The oscillators of interest (a representative device is shown in Figure 1) are composed of three major components: non-interdigitated comb-drive actuators (A,B), flexures (C), and backbone (D). To actuate these devices an AC signal is applied to a single set of comb-drives. For tuning purposes a DC signal can be applied to a second set of electrodes [4]. Due to the unique geometry of non-interdigitated comb-fingers, a time varying force is produced when an AC signal is applied, which ultimately gives rise to the parametric excitation of these devices. The nonlinear Mathieu Equation for a general device without tuning describes the dynamics of interest,

$$m\ddot{x} + c\dot{x} + k_1x + k_3x^3 + (r_{1A}x + r_{3A}x^3) V_A^2 (1 + \cos \omega t) = 0, \quad (1)$$

where, k_1 and k_3 are respectively the linear and cubic nonlinear mechanical stiffness of the flexures, r_{1A} and r_{3A} are respectively the linear and cubic nonlinear electrostatic stiffness of the non-interdigitated comb-fingers, m is the mass, V_A is the excitation voltage amplitude of a square-root cosine signal, and c is the damping coefficient. It is important to note that a square-root cosine signal is applied to the device to isolate harmonic and parametric excitation [3]. For more information on the derivation of this governing equation, see [10]. For filtering applications a second set of comb-drives is added, to which a DC signal is applied for tuning purposes [6]. The analysis in [10] deals with a generalized equation, which can be applied to devices with or without this DC set of comb-fingers. The time varying electrostatic forcing terms of Equation (1) lead to both linear and nonlinear parametric excitation, which creates the rich dynamics described in [10].

B. Analysis and Verification

In [10], a perturbation technique known as averaging was employed to study Equation (1). Specifically, the second order nonautonomous system was transformed into two first order autonomous equations in amplitude and phase form. The amplitude and phase equations are coupled by a cubic nonlinear excitation parameter, which is the direct result of the nonlinear parametric term in Equation (1). As a result, the nontrivial solutions of the system become more complicated than in the case of purely linear parametric excitation. Since damping has little effect on the qualitative nature of the system's nonlinear behavior, it was taken to be zero to simplify the analysis. It was found that there are four distinct steady state solutions to the averaged equations. One is a trivial solution, for which the amplitude is equal to zero for all values of driving frequency, which we refer to as the no-motion state. The three others are nontrivial, corresponding to periodic solutions of Equation (1). As a direct result of this analysis, effective nonlinearities are defined for the system and six distinct regions in parameter space are defined, each of which harbors a distinct qualitative nonlinear behavior [10].

To verify these analytical results numerical bifurcation analysis was performed on the original equation of motion (1) in the presence of small damping. The driving frequency was treated as a bifurcation parameter and Floquet multipliers were calculated to determine the stability of the solutions. Figure 2 shows the numerically generated plot for the case of small damping, with parameter values corresponding to region IV of nonlinear parameter space in [10]. Figure 3 shows the analytical results for the averaged equations taking the same parameters, but with zero damping. See [10] for specific parameter values. In both Figure 2 and 3, the detuning axis refers to a non-dimensionalized frequency, which was scaled to measure the closeness of the driving frequency to twice the natural frequency, see [10] for further information on these figures. Numerical simulations for small damping match well with, and confirm the validity of, the analytical model that assumes zero damping. Having the recently developed analytical tools, combined with the fact that oscillators exhibiting dy-

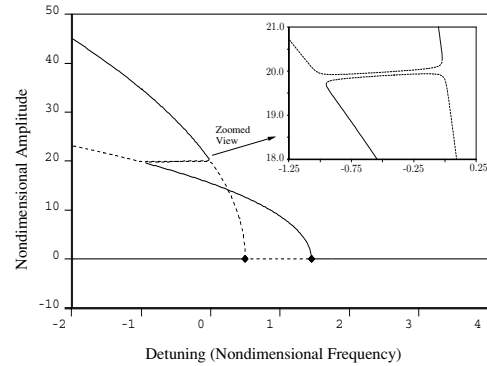


Fig. 2. Numerical bifurcation analysis of Equation (1) with small damping, where solid lines represent stable solutions and dashed lines unstable solutions. The parameters taken are described in [10] and correspond to region IV of nonlinear parameter space therein.

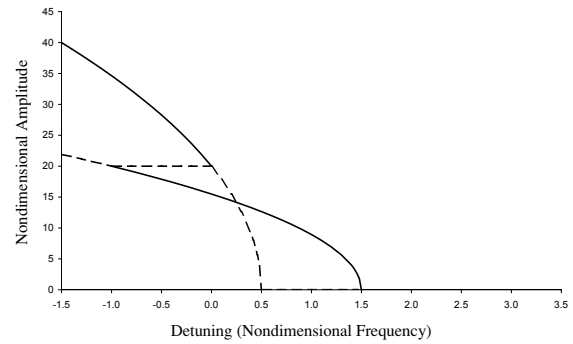


Fig. 3. Analytical bifurcation analysis of the averaged equations derived from Equation (1) with zero damping, where solid lines represent stable solutions and dashed lines unstable solutions. Apart from the damping coefficient, the same parameters as Figure 2 are used.

namics described by Equation (1) are difficult to characterize, motivates the development of a robust identification procedure, which is discussed in the following section.

II. SYSTEM IDENTIFICATION

Experimental results, first shown in [9], for a parametrically excited MEM oscillator have been obtained using a laser vibrometer [11]. The device tested has a single set of non-interdigitated comb-drives, to which a square root cosine signal is applied for actuation. Using these experimental results, analytical and numerical predictions are validated and system parameters are identified.

Theoretical stability boundaries are determined by calculating the eigenvalues of the Jacobian evaluated at the steady state solutions of the averaged equations. A stability change occurs when the real part of an eigenvalue crosses through zero. Analyzing the trivial steady state solution in the presence

of damping, the following boundaries yield zero eigenvalues:

$$f_1 = \frac{\omega_o}{2\pi} \left[2 + \frac{r_{1A}V_A^2}{k_1} - \sqrt{\left(\frac{r_{1A}V_A^2}{2k_1}\right)^2 - \frac{c^2}{mk_1}} \right], \quad (2)$$

$$f_2 = \frac{\omega_o}{2\pi} \left[2 + \frac{r_{1A}V_A^2}{k_1} + \sqrt{\left(\frac{r_{1A}V_A^2}{2k_1}\right)^2 - \frac{c^2}{mk_1}} \right], \quad (3)$$

where f_1 and f_2 are frequencies dependent on the excitation voltage V_A , and $\omega_o = \sqrt{k_1/m}$. These two boundaries define a wedge shaped zone, wherein the no-motion state transitions from being stable outside the wedge, to unstable inside the wedge. In dynamical systems language, this instability region is known as an Arnold Tongue [12]. Next, the nontrivial steady state solutions are analyzed in a similar manner, but with damping taken to be zero due to complicated Jacobian matrices. Analyzing these solutions gives rise to two distinct boundaries,

$$f_3 = \frac{\omega_o}{2\pi} \left[2 - \frac{3r_{1A}}{2k_1} \frac{k_3}{r_{3A}} - \frac{r_{1A}V_A^2}{k_1} \right] \quad (4)$$

$$f_4 = \frac{\omega_o}{2\pi} \left[2 - \frac{3r_{1A}}{2k_1} \frac{k_3}{r_{3A}} \right], \quad (5)$$

at which bifurcations, associated with saddle-node bifurcations for the case of small damping, occur. Notice that f_4 is not dependent on the excitation voltage; this is not the case in the presence of damping, yet it still gives a good approximation of the boundary location for small damping.

To identify system parameters Equations (2) and (3) are considered first, since these boundaries are solely dependent on linear parameters, k_1 , r_{1A} , c , and m . Using a nonlinear least squares fitting method, experimental data for the actual device is fit to the theoretical Arnold Tongue. Approximations for each parameter are determined in software packages, such as ANSYS, to act as first guesses for the fit. Linear parameters for the actual device are found to be, $k_1 = 2.85 \mu\text{N}/\mu\text{m}$, $r_{1A} = 2.96 \times 10^{-3} \mu\text{N}/\text{V}^2 \mu\text{m}$, $c = 3.88 \times 10^{-8} \text{kg}/\text{s}$, and $m = 9.93 \times 10^{-11} \text{kg}$. The theoretical wedge for these parameters matches the experimental results very well; Figure 4 shows the numerically determined Arnold Tongue, labeled AT, and experimental Arnold Tongue, represented by diamonds.

Knowing the four linear parameters, the last two nonlinear parameters are estimated using a similar technique. A nonlinear least squares method is used to fit Equations (4) and (5) to experimentally determined saddle-node bifurcations. Since both equations depend on k_3/r_{3A} , this ratio is determined from such a fit to be -455.7V^2 . Unfortunately, the experimental saddle-node boundaries do not match well with the theoretical boundaries in this case, but it serves as a good first approximation. So, additional information is used to improve the fit. Qualitative changes in the systems' nonlinear response have been predicted to occur at the following transition voltages [10],

$$V_{A,C1} = \sqrt{\frac{-3k_3}{5r_{3A}}}, \quad V_{A,C2} = \sqrt{\frac{-3k_3}{r_{3A}}} \quad (6)$$

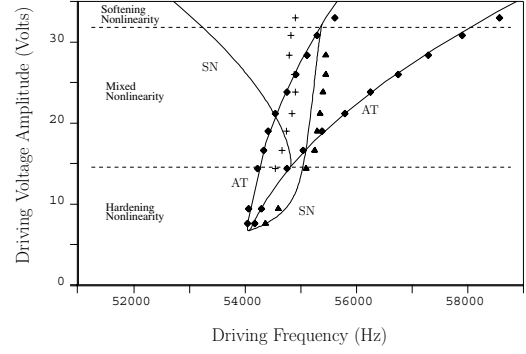


Fig. 4. Two parameter plot, voltage amplitude versus excitation frequency, mapping out numerical and experimental instability boundaries. Lines labeled AT and SN are respectively the Arnold Tongue and the curve along which saddle-node bifurcations of periodic orbits occur, as obtained by numerical bifurcation analysis of Equation (1). Symbols indicate the experimental results, with diamonds giving the location of the Arnold Tongue and pluses and triangles giving the location of saddle-node bifurcations

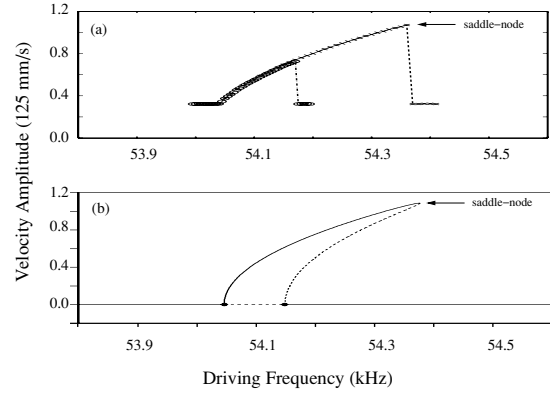


Fig. 5. Experimental and numerical responses for drive amplitude of 7.6V are depicted in (a) and (b), respectively. In (a), dashed lines with X's represents the response when sweeping up in frequency and dashed-dotted lines with O's represents the response when sweeping down in frequency. Bifurcations at either edge of the Arnold Tongue are indicated with diamonds in (b).

which represent the transition from a pure hardening to a mixed nonlinearity and from a mixed to pure softening nonlinearity, respectively. Using these transition voltages and numerical simulations, a ratio is determined that gives better quantitative, namely -352V^2 . Numerically determined saddle-node bifurcations, shown as solid curves labeled SN, and corresponding experimental data, labeled with pluses and triangles, are given in Figure 4. Transitions between the three nonlinear response regimes, labeled in Figure 4 with horizontal dashed lines, match well with the experimental transitions. Also, the right saddle-node bifurcation branch shows good quantitative agreement. On the other hand, the left saddle-node branch does not match as well with experimental results, therefore suggesting that further improvement is needed in the full identification of this system.

Once the ratio is determined for the nonlinear parameters, the magnitude of these parameters is chosen so that numerically generated response amplitudes are close to ex-

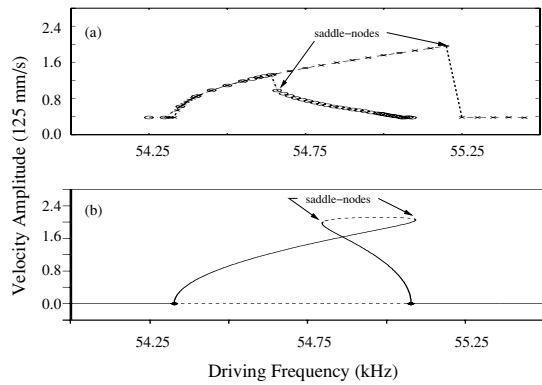


Fig. 6. Experimental and numerical responses for drive amplitude of 16.6V are depicted in (a) and (b), respectively. Conventions are the same as in Figure 5.

perimental response amplitudes. Nonlinear parameters giving reasonable correspondence between numerical simulation and experimental response amplitudes are: $k_3 = 0.075 \mu\text{N}/\mu\text{m}^3$ and $r_{3A} = -2.1 \times 10^{-4} \mu\text{N}/\text{V}^2 \mu\text{m}^3$. Figures 5(a) and 5(b) depict an experimentally and numerically generated response when driving the oscillator with a 7.6V amplitude square root cosine signal, respectively. Notice, the parameters determined with this procedure result in a theoretical response that predicts the actual response of the device with reasonable accuracy. Figures 6(a) and 6(b) depict an experimentally and numerically generated response when driving the oscillator with a 16.6V amplitude square root cosine signal, respectively. At this voltage, the theory predicts the frequency at which each bifurcation occurs with reasonable accuracy and, qualitatively speaking, captures the mixed nonlinear nature nicely; however, it does not fully agree with the experimental results. For example, the amplitude of the right saddle-node bifurcation in Figure 6(b) is close in value to the right saddle-node bifurcation in Figure 6(a), but the left saddle-node bifurcation in Figure 6b occurs at a much higher amplitude than Figure 6(a). In fact, in Figure 4, it is evident that the left saddle-node bifurcation deviates more from the experimental results as the voltage is increased. This suggests that higher order nonlinearities might need to be included into the model to more accurately capture the dynamics of this type of device. Inconsistencies between experiment and theory may also be due to the presence of noise in the experiment, which is not taken into account in the model. The basin of attraction for stable periodic solutions may be small enough for noise to perturb the oscillator into the no-motion basin of attraction, before the theoretical saddle-node bifurcation is reached [13].

III. CONCLUSION

A generalized model for the dynamics of electrostatically driven nonlinear parametric MEM oscillators has been developed. Until now, studies have only grazed the surface of the rich dynamics inherent to this system. Analytical studies, for the case of zero damping, have been verified with numerical simulations, for the case of small damping. These analytical

results will ultimately serve as useful tools for designers creating filters [6], mass sensors [5], and many other devices where a high degree of sensitivity is desired. The set of six system parameters have been characterized for an actual parametrically excited MEMS device. Fitting experimental data to theoretical boundaries for the Arnold Tongue produces accurate estimates for the system's linear parameters, k_1 , r_{1A} , c , and m . To determine a ratio between the nonlinear parameters, experimental data is fit to theoretical saddle-node bifurcation boundaries. This ratio is then optimized using theoretical transitions between various qualitative regions of the nonlinear response. Numerical simulations reveal that further improvements need to be made to the model and possibly the experiment. For instance including higher order nonlinearities in the model would improve system identification, but it would also complicate the analysis drastically. Overall, the parameters chosen capture the dynamics of the oscillator well qualitatively, and for the most part quantitatively.

ACKNOWLEDGMENT

The work was supported by the Air Force Office of Scientific Research under contract F49620-02-1-0069 and by the National Science Foundation under grant NSF-0428916. The authors would also like to thank Mike Northern for taking the SEM image shown and Mike Requa for editing this paper.

REFERENCES

- [1] D. Rugar and P. Grutter, "Mechanical parametric amplification and thermomechanical noise squeezing," *Physical Review Letters*, vol. 67 (6), pp. 699–702, 1991.
- [2] M. Napoli, W. Zhang, K. Turner, and B. Bamieh, "Characterization of electrostatically coupled microcantilevers," *Journal of Microelectromechanical Systems*, vol. 14 (2), pp. 295–304, 2005.
- [3] K. Turner, S. Miller, P. Hartwell, N. MacDonald, S. Strogatz, and S. Adams, "Five parametric resonances in a microelectromechanical system," *Nature*, vol. 396, pp. 149–152, 1998.
- [4] S. Adams, F. Bertsch, and N. MacDonald, "Independent tuning of linear and nonlinear stiffness coefficients," *Journal of Microelectromechanical Systems*, vol. 7 (2), pp. 172–180, 1998.
- [5] W. Zhang, R. Baskaran, and K. Turner, "Effect of cubic nonlinearity on auto-parametrically amplified resonant MEMS mass sensor," *Sensors and Actuators A-Physical*, vol. 102 (1-2), pp. 139–150, 2002.
- [6] J. Rhoads, S. Shaw, K. Turner, and R. Baskaran, "Tunable MEMS filters that exploit parametric resonance," *ASME Journal of Vibration and Acoustics*, vol. 127 (5), pp. 423–430, 2005.
- [7] A. H. Nayfeh and D. T. Mook, *Nonlinear Oscillations*. New York: Wiley-Interscience, 1977.
- [8] R. Zouanes and R. Rand, "Subharmonic resonance in the non-linear Mathieu equation," *International Journal Non-linear Mechanics*, vol. 37, pp. 43–73, 2002.
- [9] W. Zhang, R. Basharan, and K. Turner, "Tuning the dynamic behavior of parametric resonance in a micromechanical oscillator," *Applied Physics Letters*, vol. 82 (1), pp. 130–132, 2003.
- [10] J. Rhoads, S. Shaw, K. Turner, J. Moehlis, B. DeMartini, and W. Zhang, "Generalized parametric resonance in electrostatically-actuated microelectromechanical oscillators," *Submitted to the Journal of Sound and Vibration*, 2005.
- [11] K. Turner, P. Hartwell, and N. MacDonald, "Multi-dimensional MEMS motion characterization using laser vibrometry," in: *Transducers 1999 The Tenth International Conference on Solid-State Sensors and Actuators*, pp. 1144–1147, 1999.
- [12] S. Wiggins, *Introduction to Applied Nonlinear Dynamical Systems and Chaos*, 2nd ed. New York: Springer-Verlag, 2003.
- [13] J. Aldridge and A. Cleland, "Noise-enabled precision measurements of a Duffing nanomechanical resonator," *Physical Review Letters*, vol. 94, 2005, article number 156403.